



A comparative study on mechanical polishing and laser polishing of laser-nitrided Zr-based metallic glass surface

Jing Hong¹ · Lin Zhang² · Zhiyu Zhang³ · Hu Huang¹ · Jiwang Yan²

Received: 16 August 2022 / Accepted: 12 November 2022 / Published online: 26 November 2022
© The Author(s), under exclusive licence to Springer-Verlag London Ltd., part of Springer Nature 2022

Abstract

As a promising surface modification method, nanosecond pulsed laser nitriding has been widely employed in enhancing the surface hardness and chemical corrosion of Zr-based metallic glass (MG). However, laser nitriding generally leads to poor finished surface quality, limiting its potential applications. For flattening the laser-nitrided surface, the most common methods, i.e., mechanical polishing (MP) and a novel proposed flattening approach, laser polishing (LP), were comparatively studied. A systematical comparison between MP and LP on three types of laser-nitrided surfaces was performed to evaluate the surface roughness, surface hardness, and plastic deformation. The experimental results indicate that the surface roughness of these three laser-nitrided surfaces is reduced by 56.4%, 58.1%, and 44.6% by MP. In contrast, a remarkable improvement in the surface quality is achieved with a maximum reduction in surface roughness by 80.4%, 81.5%, and 74.2% by LP, respectively. While in terms of the surface mechanical properties, the LP surfaces exhibit slightly lower hardness than the corresponding MP surfaces, which are both enhanced in hardness compared with as-cast MG. Additionally, no matter on the MP or LP surfaces, the shear bands and serrated flows have been significantly suppressed compared with as-cast MG, demonstrating that the micro-scale plastic deformation of as-cast MG has been modified. Although the obtained results indicate that the surface roughness of the laser-nitrided surface could be improved by both MP and LP, in terms of environmental friendliness, flexibility, and controllability, the LP shows dominant advantages and enormous potential in industry and consumer products.

Keywords Laser nitriding · Laser polishing · Mechanical polishing · Nanosecond pulsed laser · Zr-based metallic glass

1 Introduction

Due to their excellent properties, such as relatively high strength, hardness, and superior resistance to mechanical wear and chemical corrosion [1–3], metallic glasses (MGs) are expected to open up new application opportunities in the fields of aerospace, precision machinery, military weapons, and so on [4–6]. However, the poor tensile plasticity of most MGs at room temperature restricts their applications as structural and engineering materials [7–9]. Despite this, the high surface hardness of MGs, compared with their crystalline alloy counterparts, provides several potential applications as surface functional materials. Thus, employing appropriate machining approaches to improve surface hardness is meaningful for further extending the functional applications of MGs in the fields of biomedicine and tribology.

Laser nitriding is commonly recognized as one of the most promising approaches to improving the surface properties of materials, such as surface hardness and wear

✉ Lin Zhang
zhanglin@keio.jp

✉ Hu Huang
huanghu@jlu.edu.cn

¹ School of Mechanical and Aerospace Engineering, Electron Microscopy Center, Jilin University, Changchun, Jilin 130022, China

² Department of Mechanical Engineering, Faculty of Science and Technology, Keio University, Yokohama 223-8522, Japan

³ Key Laboratory of Optical System Advanced Manufacturing Technology, Fine Mechanics and Physics, Changchun Institute of Optics, Chinese Academy of Sciences, Changchun, China

resistance [10–14]. As reported in the previous research [15], the surface hardness of Zr-based MG could be significantly improved by laser nitriding due to the formation of ZrN. However, accompanied by this process, some surface defects, such as surface fluctuations, peaks, and valleys, are generated on the laser-nitrided MG surface simultaneously, resulting in poor surface quality and significantly hindering its practical applications. Therefore, high-quality polishing treatment is urgently required for flattening the laser-nitrided MG surface.

Traditional flattening approaches generally include electrochemical, chemical, and mechanical polishing treatments [16–18] as well as the vibration or electromagnetic-assisted polishing methods [19–22], among which mechanical polishing (MP) is the most commonly used due to the optical-level smoothness and excellent flatness of the polished surface with easy operation and simple apparatus. Although MP is still dominant, a novel flattening approach, i.e., laser polishing (LP), has been proposed recently. Compared with the conventional methods, this approach ensures the possibility of less machining time, focusing on the selected localized region, and no tool wear and chemical pollution [23–27]. However, despite these benefits, some challenges still exist for those mentioned above two flattening approaches. For MP, low processing efficiency and unsuitability for complex shapes hinder its application, while for LP, the thermal shock introduced might alter the properties of the sample subsurface, affecting material structures and surface properties. The above analysis indicates that both MP and LP have their own advantages and disadvantages, and their applicability for flattening the laser-nitrided MG surface should be further explored. In this manuscript, both MP and LP on three types of laser-nitrided Zr-based MG surfaces were performed. The resultant surface characteristics were comparatively analyzed in terms of surface morphology, roughness, hardness, and plastic deformation. Finally, the mechanism in LP was introduced based on the above experiments, which might provide some reference for further studies on LP.

2 Materials and experiments

2.1 Materials

A typical metallic glass block ($Zr_{41.2}Ti_{13.8}Cu_{12.5}Ni_{10}Be_{22.5}$) with the dimension of 20 mm × 20 mm × 2 mm was used. Prior to laser irradiation, the Zr-based MG was mechanically ground with 400, 800, 1200, and 2000 grit sandpapers, followed by mechanical polishing with the diamond abrasive paste by a commercial polishing machine (UNIPOL-802, MTI Corporation, China). Finally, the sample was cleaned with alcohol to remove the residual chips and abrasives on the surface.

2.2 Preparation of laser-nitrided MG surfaces

For preparing the laser-nitrided MG surfaces, laser irradiation of the smooth MG surface was performed in a nitrogen atmosphere by a fiber nanosecond pulsed laser system (SP-050P-A-EP-Z-F-Y, SPI Lasers, UK) with a pulse duration of 10 ns and a repetition frequency of 600 kHz. This laser system produces near-infrared light with a central wavelength of 1064 nm. According to some preliminary experiments [14], the laser power and overlap rate were selected as 3.8 W and 70%, respectively. To obtain different laser-nitrided surfaces with variable surface micro-structures, two kinds of scanning speeds were employed (10 mm/s and 20 mm/s), and the number of irradiation cycles was determined as 1 and 4 for the case of 10 mm/s. Under these experimental conditions, three types of laser-nitrided surfaces with the dimension of 2 mm × 2 mm were obtained, which were defined as surfaces A, B, and C. For comparison, surfaces A, B, and C were prepared on the same sample. The laser irradiation parameters in laser nitriding are listed in Table 1.

2.3 Surface flattening treatments

2.3.1 MP process

After laser nitriding, MP was performed on the three laser-nitrided surfaces, and the schematic diagram is shown in Fig. 1. First of all, the nitrided sample is placed on a polishing cloth, which is attached to a polishing plate with a thickness of 50 mm and diameter of 300 mm. Then, the polishing plate rotates with the angular speed of 80 r/min for 3600 s, and the protruding defects from the surface are gradually removed by the dispersed diamond abrasives with the size of 0.5 μm under a normal load of 0.5 kg. Notably, in the process of mechanical polishing, it is necessary to observe the polishing effect of the laser-nitrided surfaces every 5 mins and reapply the diamond abrasives to the laser-nitrided surfaces.

2.3.2 LP process

For LP of the laser-nitrided surfaces, the same nanosecond pulsed laser was employed. In order to prevent the sample

Table 1 Laser irradiation parameters for preparing three laser-nitrided surfaces A, B, and C

	Laser power (W)	Scanning speed (mm/s)	Number of irradiation cycle	Overlap rate (%)
Surface A	3.8	20	1	70
Surface B	3.8	10	1	70
Surface C	3.8	10	4	70

Fig. 1 Schematic diagram of MP process on laser-nitrided surfaces

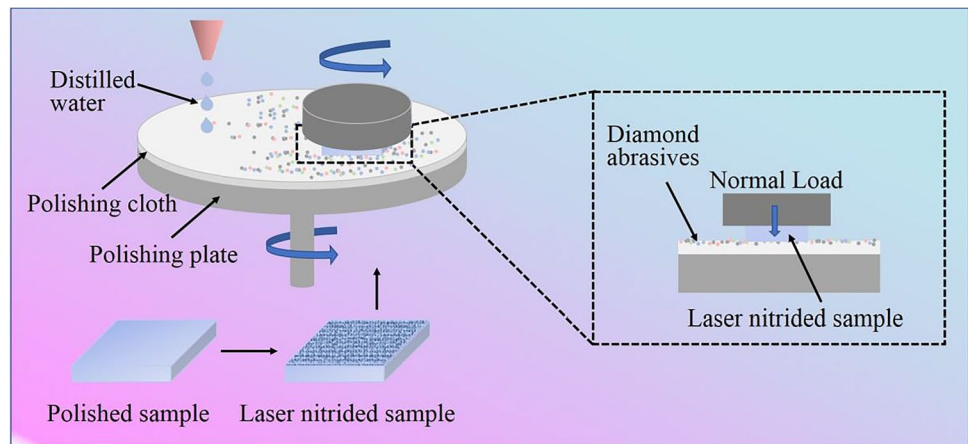
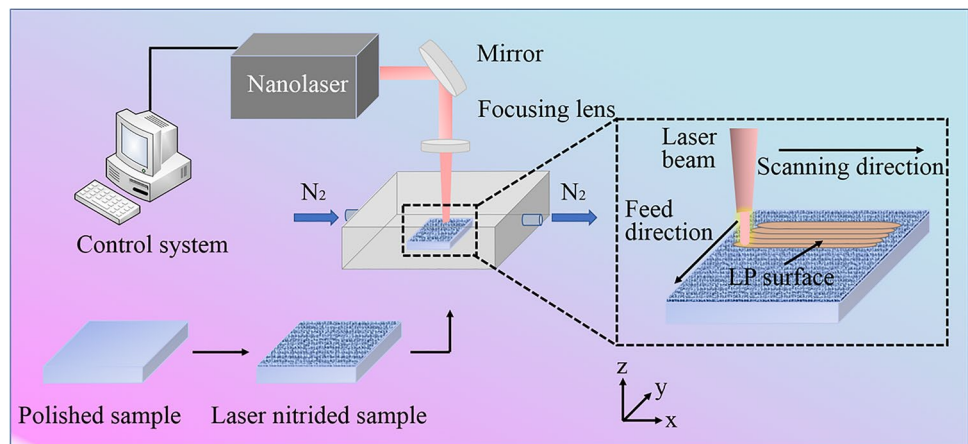


Fig. 2 Schematic diagram of LP process on laser-nitrided surfaces



surface from oxidization, LP was performed in the chamber filled with nitrogen gas. The schematic diagram of the LP process on laser-nitrided surfaces is illustrated in Fig. 2. The laser beam is focused on the laser-nitrided surface with an F-theta lens and scans at the speed of 300 mm/s. After single-line irradiation, the laser beam is shifted by 9.2 μm concerning the previous scanning track (overlap rate of 80%). To investigate the influence of laser power on LP, various laser powers (5.4, 7.1, and 8.8 W) were selected, as listed in Table 2. The processing time of LP with different laser parameters is approximately 0.01 s.

2.4 Characterization

The SEM morphologies of the laser-nitrided surfaces before and after flattening treatments (MP and LP) were captured via the tungsten filament scanning electron microscope (SEM, JSM-IT500A, JEOL, Japan). The acceleration voltage and working distance (WD) were set as 10.0 kV and 11.5 mm, respectively. The three-dimensional (3D) morphologies and surface roughness corresponding to SEM morphologies were measured by the laser scanning confocal microscope (LSCM, OLS4100, Olympus, Japan). The

Table 2 Laser irradiation parameters for LP on laser-nitrided surfaces A, B, and C

LP parameter	Value
Laser power (W)	5.4, 7.1, 8.8
Scanning speed (mm/s)	300
Overlap rate (%)	80

surface hardness of the laser-nitrided surfaces after flattening treatments (MP and LP) was characterized by a nanoindentation instrument (DUH-211, SHIMADZU, Japan) with a pyramidal indenter (pyramidal indenter with an angle of 115° between the ridge and face, Tokyo Diamond Tools MFG. Co., Ltd., Japan). During the nanoindentation tests, the indentation load and the loading rate were set as 120 mN and 10 mN/s, respectively. The crystalline phases of the local regions on the laser-nitrided surfaces before and after flattening treatments (MP and LP) were obtained via an X-ray diffractometer (XRD, D8 Discover, Bruker, Germany) with a two-dimensional (2D) detector. Phase identification was performed with the 2θ angle between 20° and 80° with rocking detection mode.

3 Results and discussion

3.1 Morphologies of laser-nitrided surfaces

Figure 3 illustrates the SEM morphologies of surfaces A, B, and C. To further evaluate the surface quality, the corresponding 3D morphologies are obtained and the corresponding 2D profiles perpendicular to the scanning direction are extracted as insets. From the results, it is observed that all three laser-nitrided surfaces are covered by numerous protruding peaks and deep valleys, and their spatial fluctuations together with the height difference between peaks and valleys (PV value) are increased in the order of surfaces A, B, and C, which should be attributed to the stronger interaction between laser and MG with the increased irradiation energy and scanning cycles. Furthermore, the crystalline phases of surfaces A, B, and C were characterized by XRD. For comparison, the as-cast MG was also included. As illustrated in Fig. 4, the diffraction peaks of the ZrN phase are clearly observed in the XRD patterns of surfaces A, B, and C, which are remarkably different from the amorphous characteristics of as-cast MG. Furthermore, the peak intensity of the ZrN phase tends to gradually increase in the order of surfaces A, B, and C, which indicates that the amount of ZrN phase generated during laser nitriding is enhanced with the increased irradiation energy and scanning cycles. Nevertheless, these three laser-nitrided surfaces exhibit irregular and rough

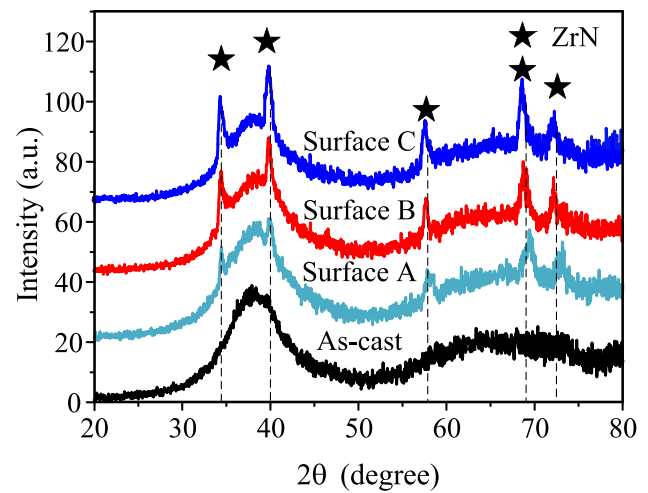


Fig. 4 XRD patterns obtained for the as-cast MG and laser-nitrided surfaces A, B, and C

morphologies. Therefore, post-processing is required to flatten the laser-nitrided surfaces.

3.2 Surface morphologies after MP and LP

3.2.1 Surface morphologies after MP

Figure 5 illustrates the SEM morphologies of surfaces A, B, and C after the MP process (named MPA, MPB, and MPC).

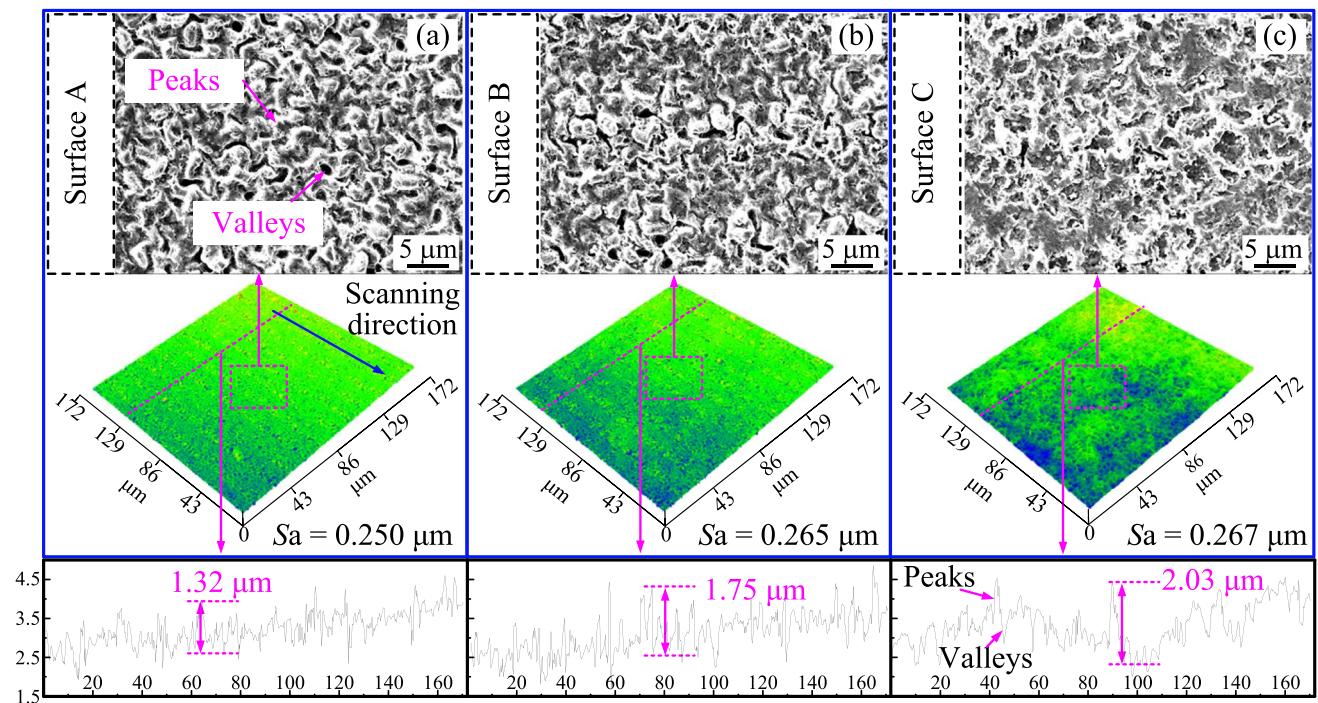


Fig. 3 SEM morphologies, 3D morphologies, as well as 2D cross-section profiles of laser-nitrided **a** surface A, **b** surface B, and **c** surface C

Compared with the initial laser-nitrided surfaces shown in Fig. 3, most protruding peaks are removed from the surfaces after MP, and some smooth regions are formed between the valleys (as shown in Fig. 5b, e, h). However, some micro-holes still remain on the polished surfaces, including MPA, MPB, and MPC. This is owing to the fact that the thickness of the material removal layer in MP is less than the partial PV values of the laser-nitrided surfaces. In addition, the distribution and dimension of the residual micro-holes on the MPA, MPB, and MPC surfaces possess variable appearances. For further understanding of the characteristics of the residual micro-holes, the surface porosity of MPA, MPB, and MPC surfaces is analyzed through image processing, and the corresponding results are shown in Fig. 5c, f, i, respectively. On the MPA and MPB surfaces, the micro-holes are uniformly dispersed on the polished surface with

the surface porosity of 16.55% and 14.73%. For the MPC surface, although the surface porosity is further reduced to 14.31%, the micro-holes are mainly concentrated in the local regions of the polished surfaces, accompanied by the increase in the size of some local micro-holes. This may be due to the increased number of irradiation cycles leading to severe ablation of the materials in some local regions. Nevertheless, the surface smoothness of surfaces A, B, and C has been significantly improved by MP compared with the initial laser-nitrided surfaces.

3.2.2 Surface morphologies after LP

Figure 6 illustrates the SEM morphologies of surfaces A, B, and C treated by the LP process (named LPA, LPB, and

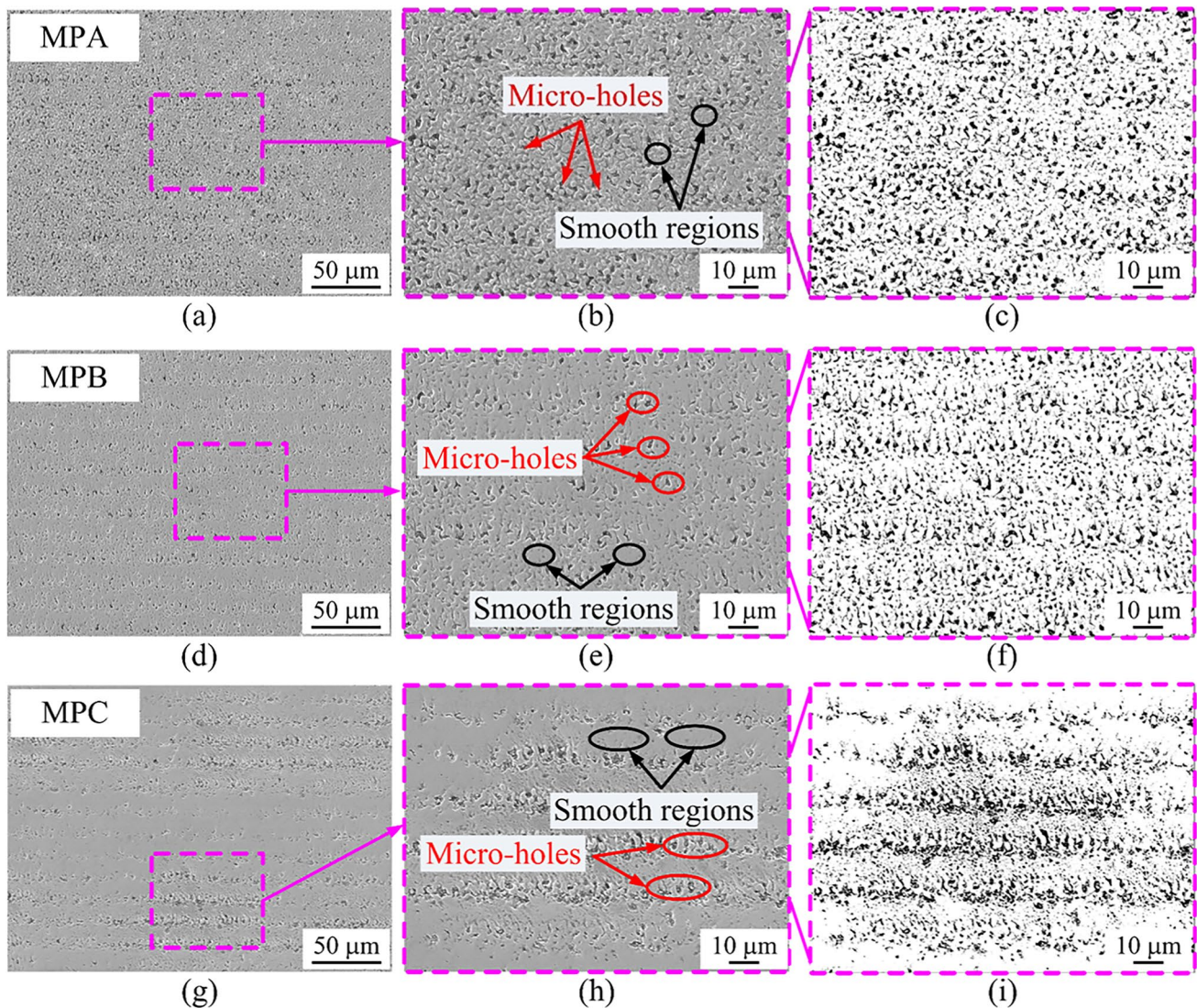


Fig. 5 SEM morphologies of the laser-nitrided surfaces after MP: **a, b** MPA, **d, e** MPB, and **g, h** MPC. Figure 5c, f, and i are the processed binary images of Fig. 5b, e, and h, respectively

LPC). From the results, the smoothness of the LP surfaces is much better than that of the MP surfaces, and some different surface characteristics occur on the LP surfaces. For instance, the surface defects, including the peaks and valleys on surfaces A, B, and C, could be completely removed with the laser powers of 5.4, 7.1, and 8.8 W, and some nano-scale surface ripples exist between the adjacent scanning tracks. Being similar to the MP surfaces, the LPA, LPB, and LPC surfaces obtained at the laser power of 5.4 W are given as an example to analyze the surface porosity, and the processed images are shown in Fig. 6d, h, and l. Accordingly, the surface porosity of the LPA, LPB, and LPC surfaces is 7.55%, 5.85%, and 1.74%, respectively, which is less than that of the corresponding MP surfaces. In general, the obtained results indicate the advantages of LP over MP in improving the surface quality of laser-nitrided surfaces.

3.3 Surface roughness after MP and LP

3.3.1 Three-dimensional morphologies and surface roughness

In order to quantitatively evaluate the effect of MP and LP, the surface roughness of the MP and LP surfaces was

measured, and the areal topography surface roughness (S_a) was determined as the evaluation index, and its formula is defined as [28],

$$S_a = \frac{1}{N_x N_y} \sum_{j=1}^{N_y} \sum_{i=1}^{N_x} |z(x_i, y_j)| \quad (1)$$

where z stands for the surface height at different spatial locations of 3D surface morphology, and N_x and N_y are the numbers of spatial locations in the x - and y -direction, respectively.

Figure 7 illustrates the 3D surface morphologies and roughness (S_a) of MPA, MPB, and MPC surfaces. It is observed that after MP, the surface roughness of surfaces A, B, and C is reduced from 0.250, 0.265, and 0.267 μm to 0.109, 0.111, and 0.148 μm , and the reduction in surface roughness is 56.4%, 58.1%, and 44.6%, respectively. Figure 8 illustrates the 3D surface morphologies and corresponding roughness (S_a) of LPA, LPB, and LPC surfaces obtained at the laser powers of 5.4, 7.1, and 8.8 W. For the LPA, LPB, and LPC surfaces, the maximum reduction in surface roughness is 80.4% (from 0.250 to 0.049 μm), 81.5% (from 0.265 to 0.049 μm), and 74.2% (from 0.267 to 0.069 μm), respectively.

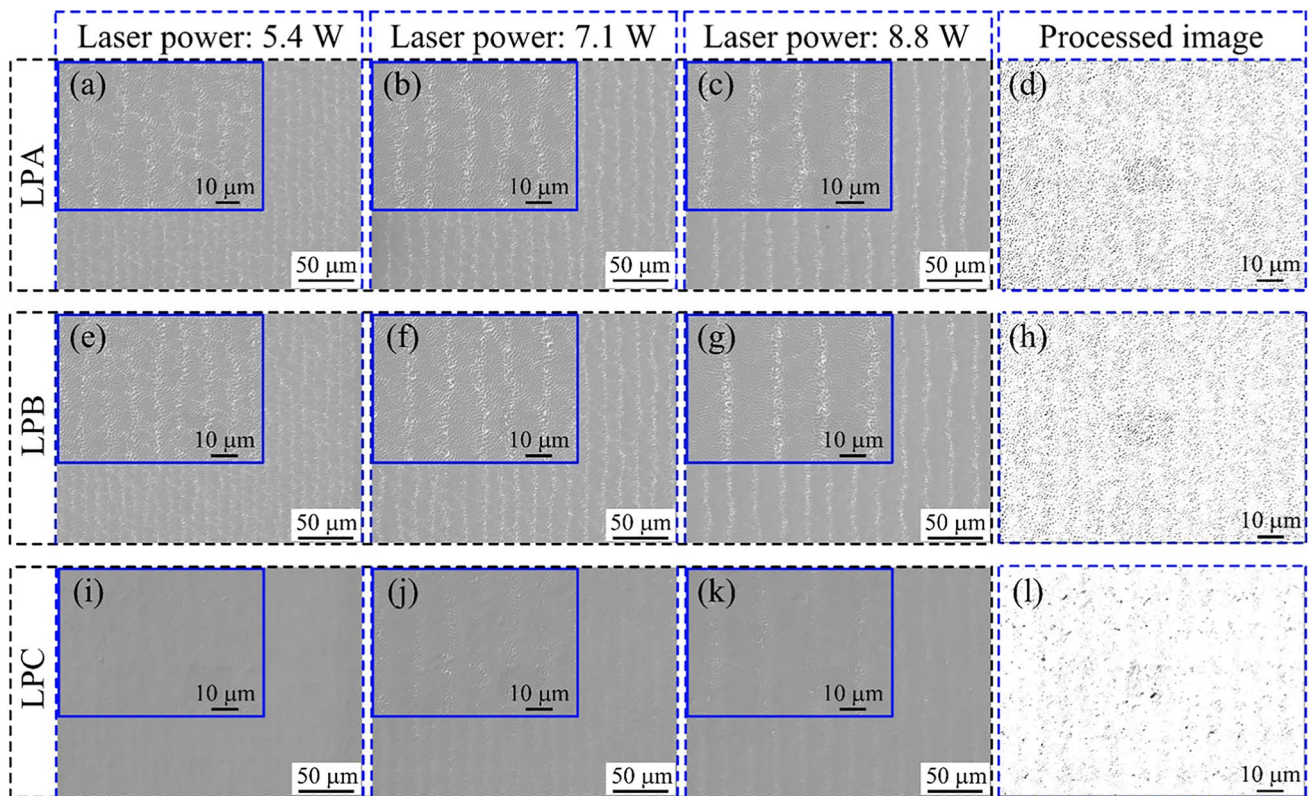


Fig. 6 SEM morphologies of the laser-nitrided surfaces after LP with three laser powers: **a–c** LPA, **e–g** LPB, and **i–k** LPC. Figure 6d, h, and l are the processed binary images of Fig. 6a, e, and i, respectively

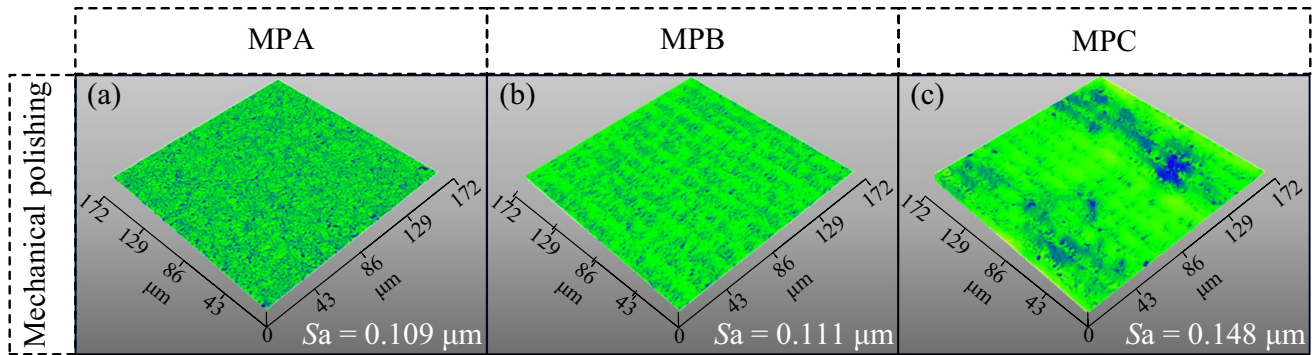


Fig. 7 3D surface morphologies of the laser-nitrided surfaces after MP: a MPA, b MPB, and c MPC

3.3.2 Potential mechanism of MP and LP

Although both MP and LP could improve the surface roughness of the laser-nitrided surfaces, the residual morphologies of the corresponding polished surfaces are completely different, which might be related to the mechanism of these two polishing treatments. The mechanism of MP only contains the mechanical interaction between the laser-nitrided surfaces

and the diamond abrasives, as illustrated in Fig. 9. When the polishing plate rotates relative to the laser-nitrided surfaces, the shear force and normal load drive numerous diamond abrasives scratching on the laser-nitrided surfaces, as shown in Fig. 9b. Accordingly, the protruding peaks from the laser-nitrided surfaces are removed at the nano/micro-scale, leading to the flattening of the nitrided surfaces. Although this method could reduce the surface roughness, the deep valleys

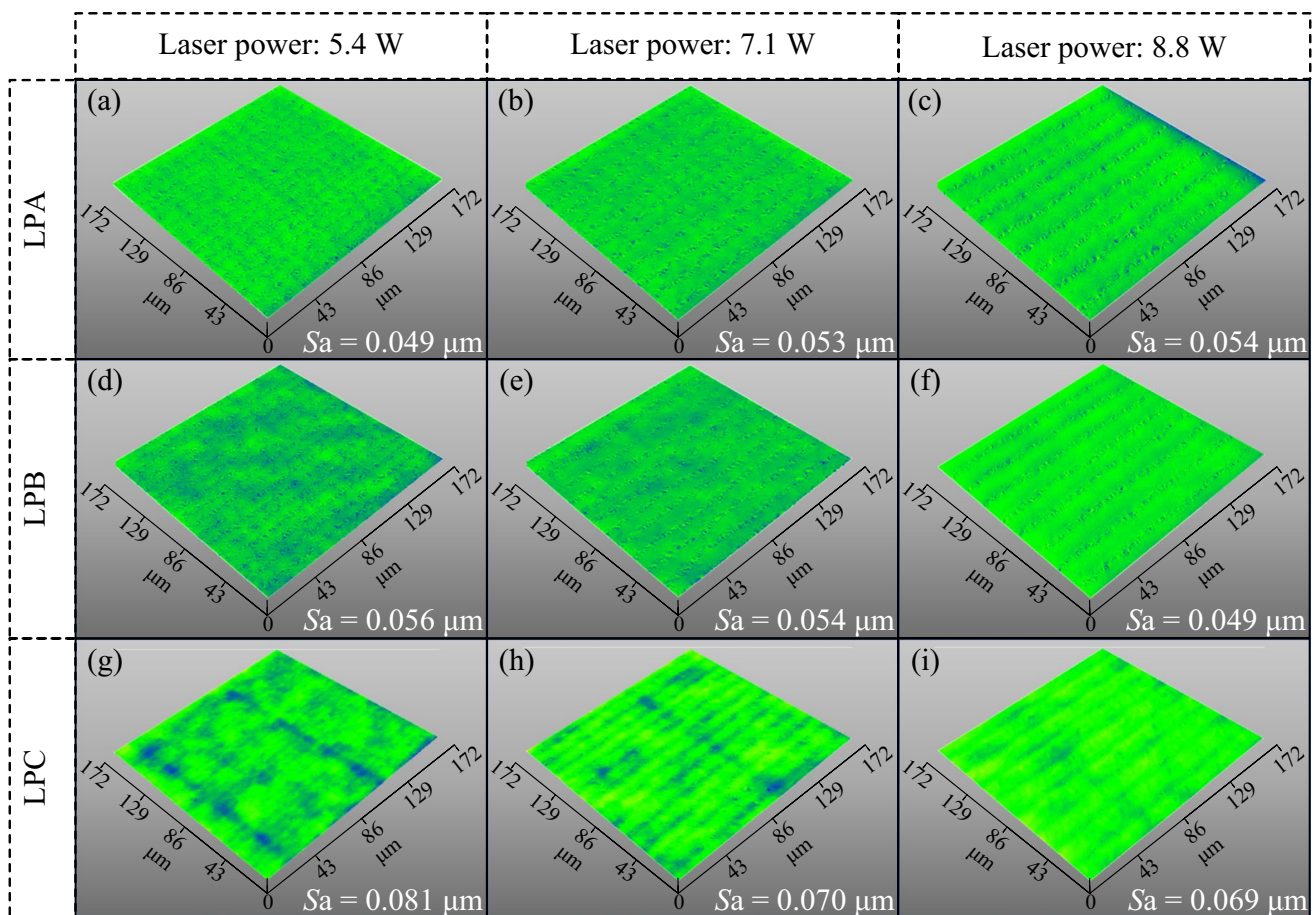


Fig. 8 3D surface morphologies of the laser-nitrided surfaces after LP with various laser powers: a–c LPA, d–f LPB, and g–i LPC

on the laser-nitrided surfaces are hardly uniformly removed, considering the micro-meter thickness of the laser-nitrided layer. Therefore, some micro-holes are observed on the MP surface, as shown in Figs. 5 and 7. In addition, some potential influence factors in MP, such as sample tilt or uneven pressure, may result in manufacturing defects.

In comparison, the interaction between laser and MG during LP involves complex physical processes, which mainly include heat transfer, re-melting, and solidification of surface materials [29, 30], and the schematic diagram of the mechanism of LP is shown in Fig. 10. Firstly, laser-nitrided surface undergoes heat transfer when irradiated by the laser beam, which causes temperature increment in the irradiated region, as shown in Fig. 10 (b1). Accordingly, when the temperature of the irradiated region is further increased, the materials in the irradiated region are melted, leading to a molten pool. The liquid materials tend to re-distribute to a smooth surface under the gravity, surface tension, and recoil pressure, as shown in Fig. 10 (b2) [31], in which the deep valleys left on the initial laser-nitrided surfaces are filled with re-melted material. As the laser beam moves along the

laser scanning direction, the temperature in the irradiated region drops sharply, forming a flat surface, as illustrated in Fig. 10 (b3).

Based on the mechanism of LP, most of the defects on the initial laser-nitrided surfaces, especially the peaks and valleys, could be re-melted or filled up during LP under the selected laser parameters. But the removal of the spatial fluctuations strongly depends on the laser power. For instance, after performing LP on surface C at the laser power of 5.4 W, the fluctuations are visible, as shown in Fig. 8g. This may be due to the sectional re-melting of the initial traces on the nitrided surface caused by insufficient heat accumulation. With the increase in laser power, the fluctuations turn out to be mild, as shown in Fig. 8h. The further increase in the laser power leads to the elimination of the fluctuations, as shown in Fig. 8i, which indicates the heat accumulation obtained at the laser power of 8.8 W is beneficial for improving the surface quality of surface C. In general, the above analysis demonstrates that surfaces A, B, and C could be flattened through both MP and LP, but LP performs better in terms of the reduction in surface roughness and machining defects, which should be attributed to the differences in the mechanism of LP and MP.

Fig. 9 Schematic diagram of mechanism of MP on laser-nitrided surface: **a** initial laser nitrided surface, **b** diamond abrasives scratching, and **c** final finished surface

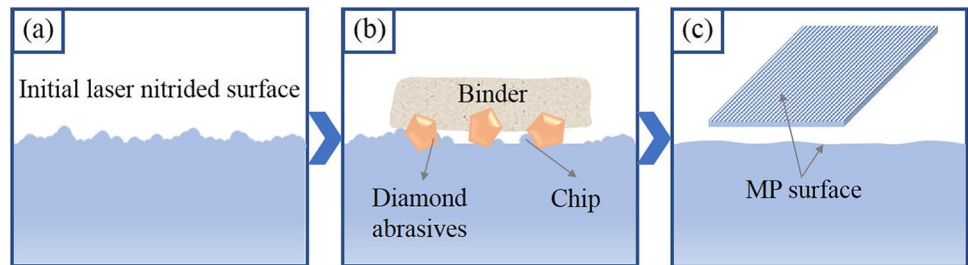
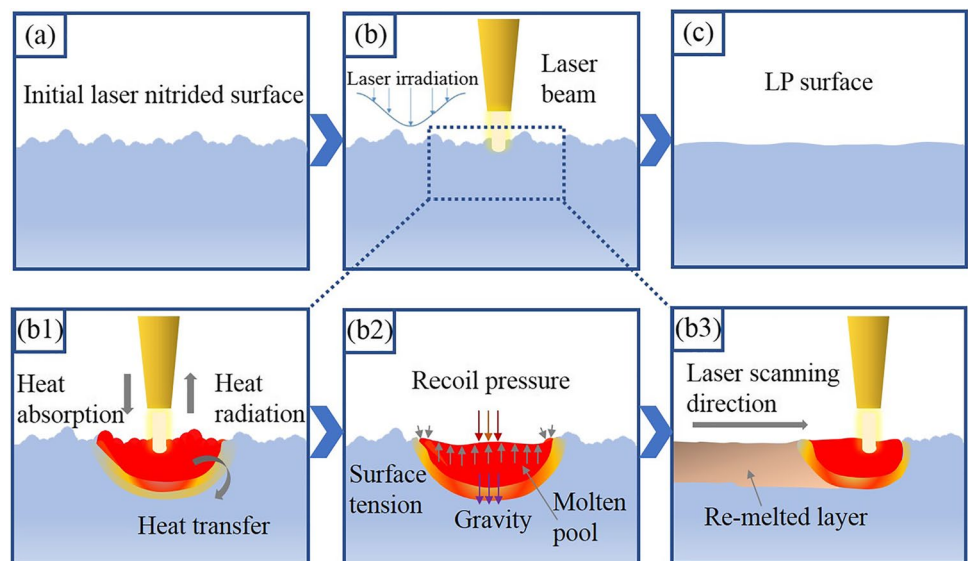


Fig. 10 Schematic diagram of mechanism of LP on laser-nitrided surface: **a** initial laser nitrided surface, **b** laser irradiation on the surface, **c** final finished surface, and **b1–b3** the detailed processes in LP



3.4 Surface hardness

For further evaluation of the mechanical property of the laser-nitrided surfaces after MP and LP, the corresponding surface hardness is investigated. Nanoindentation tests were performed to characterize the surface hardness of the MP and LP surfaces, and the indentation load and loading rate are 120 mN and 10 mN/s, respectively. To eliminate the random error, ten nanoindentation tests were performed on each polished surface.

Figure 11 shows the average hardness and corresponding XRD results of the MPA, MPB, and MPC surfaces. As observed in Fig. 11a, the average hardness of MPA, MPB, and MPC surfaces is remarkably higher than that of the as-cast MG surface. Additionally, the surface hardness is increased in the order of MPA, MPB, and MPC, matching well with the variation trend of the peak intensity of the ZrN phase in Fig. 11b. It indicates that the ZrN phase plays a significant role in improving the surface hardness [15, 32]. Furthermore, according to the XRD patterns in Figs. 4 and 11b, it can be found that although the partial laser-nitrided layer was removed by MP, the ZrN phase still exists on the MP surfaces. Therefore, it can be concluded that compared to as-cast MG, the high surface hardness of the MP surfaces compared to the as-cast MG should be due to the ZrN phase

generated in laser nitriding, and the more vigorous intensity of the ZrN phase leads to higher surface hardness.

In comparison, the average hardness of the laser-nitrided surfaces after LP with the laser powers of 5.4, 7.1, and 8.8 W is shown in Fig. 12a. In addition, the corresponding XRD patterns obtained under the laser power of 5.4 W are illustrated in Fig. 12b. As observed in Figs. 11a and 12a, the surface hardness of LP surfaces is always less than that of MP surfaces, regardless of the laser power. However, the peak intensity of the ZrN phase for the LP surfaces is stronger than that of the corresponding MP surfaces, as shown in Figs. 11b and 12b. This phenomenon might be associated with the laser shock and ZrN phase accumulation in LP. Since the characteristics of laser polishing are rapid heating and rapid cooling of the materials, a relatively high cooling rate can typically be achieved during the laser shock process, which may result in the generation of more free volume [33–35] and thus trigger surface softening behavior. In addition, the residual stress redistributions induced by the rapid melting and cooling procedure possibly contribute to surface softening as well [35].

On the other hand, LP was conducted in a nitrogen atmosphere, which would further cause the generation and accumulation of the ZrN phase, thereby contributing to the enhancement of surface hardness and the intensity of ZrN

Fig. 11 a Surface hardness and b XRD results of the as-cast MG surface as well as MPA, MPB, and MPC surfaces

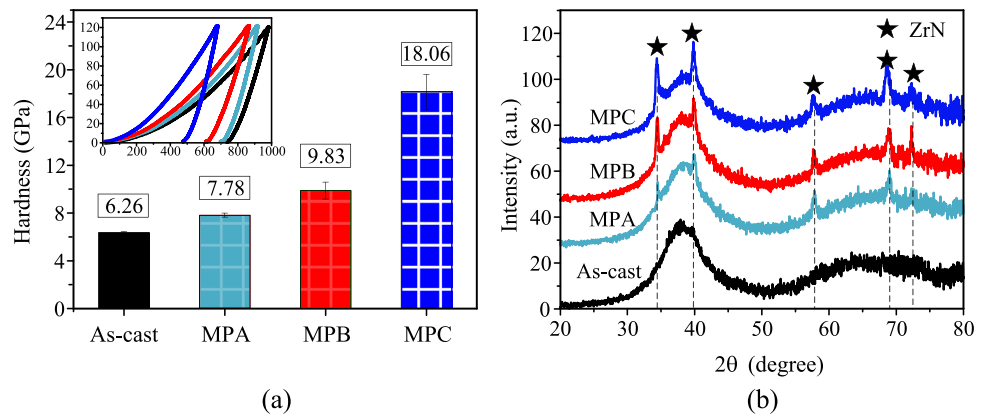
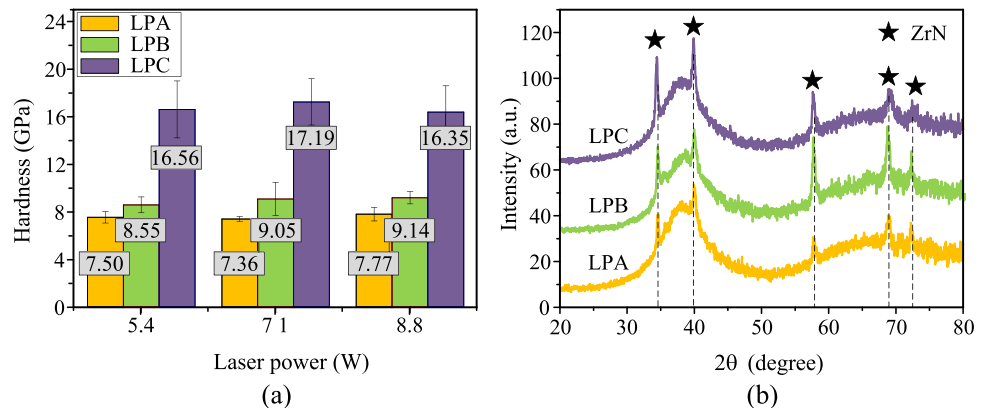


Fig. 12 a Surface hardness of the LPA, LPB, and LPC surfaces obtained at the laser powers of 5.4, 7.1, and 8.8 W. b XRD patterns obtained for the LPA, LPB, and LPC surfaces under the laser power of 5.4 W



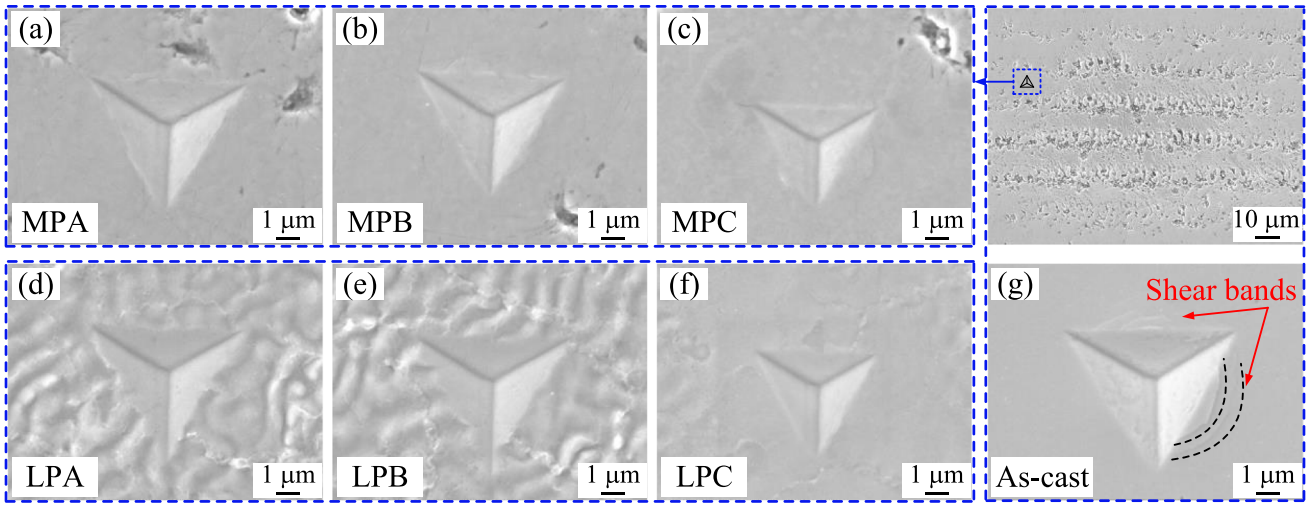


Fig. 13 SEM morphologies of residual indentations of **a–c** laser-nitrided surfaces after MP: **a** MPA, **b** MPB, **c** MPC, and **d–f** laser-nitrided surfaces after LP: **d** LPA, **e** LPB, **f** LPC, and **g** as-cast MG surface

peaks of XRD curves. Combined with the obtained results regarding surface hardness and XRD patterns, it can be concluded that during LP, the laser thermal shock shows a dominant role compared with the generation of the ZrN phase. Therefore, the LP surfaces possess a lower hardness than the MP surfaces.

3.5 Shear band and serrated flow

In addition to hardness testing, nanoindentation can also be used to evaluate the plastic deformation of surface materials. It is commonly accepted that micro-scale plastic deformation of MG could be illustrated through the occurrence of shear bands

Fig. 14 Load-depth curves and serrated flows of **a, b** laser-nitrided surfaces after MP and **c, d** laser-nitrided surfaces after LP

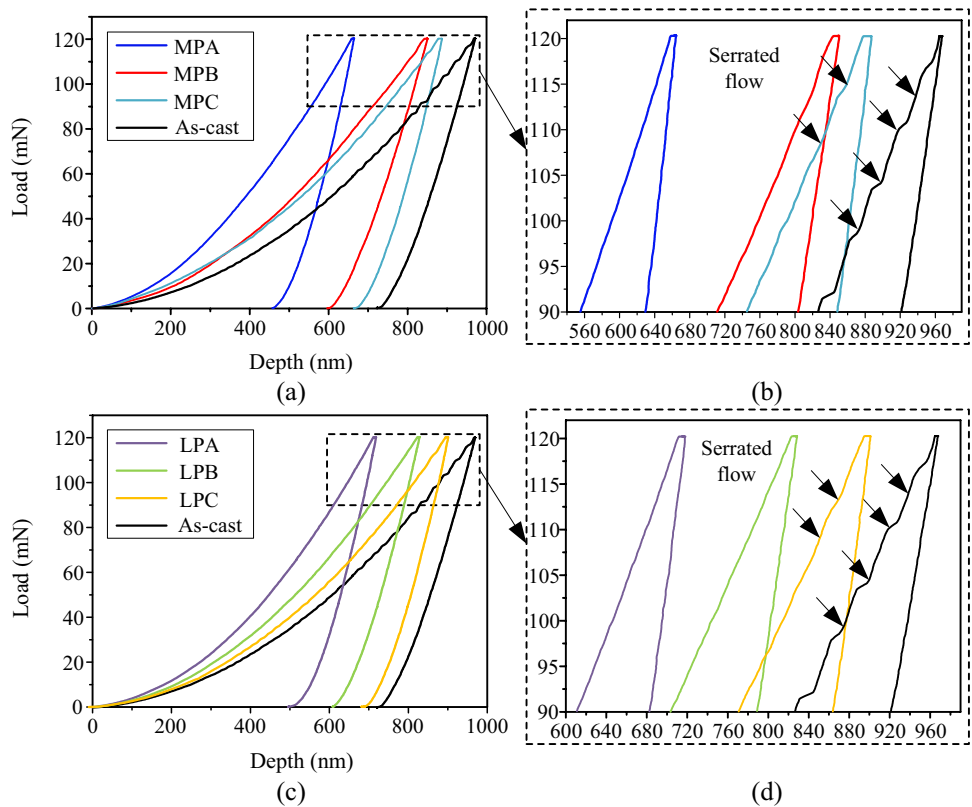


Table 3 Performance comparison of the laser-nitrided surfaces treated by MP and LP

	Laser-nitrided surface	MP	LP
Surface roughness (μm)	Surface A	0.109	0.049
	Surface B	0.111	0.056
	Surface C	0.148	0.081
Surface porosity (%)	Surface A	16.55	7.55
	Surface B	14.73	5.85
	Surface C	14.31	1.74
Surface hardness (GPa)	Surface A	7.78	7.50
	Surface B	9.83	8.55
	Surface C	18.06	16.56
Process efficiency (mm^2/s)		0.001	400

around the residual indentation [36, 37]. The SEM morphologies of residual indentations obtained on the MP and LP surfaces are shown in Figs. 13a–c and Figs. 13 d–f, respectively. For comparison, the morphology of residual indentation on the as-cast MG surface is shown in Fig. 13g, where the shear bands can be clearly observed around the residual indentation. While for the MP and LP surfaces, no shear bands are observed. The above results prove that the shear bands on both MP and LP surfaces have been significantly suppressed, which indicates that micro-scale plastic deformation of MP and LP surfaces has been altered from the initial state.

As reported in previous researches [36, 38], serrated flows are closely associated with the initiation and propagation of shear bands. The evolution of shear bands obtained above indicates that the serrated flows should have different characteristics from before. Accordingly, the load-depth curves obtained for the MP and LP surfaces under the indentation load of 120 mN and loading rate of 2 mN/s are illustrated in Fig. 14a, c, respectively. To clearly capture the characteristics of serrated flows, the locally enlarged images of the load-depth curves obtained for the MP and LP surfaces are shown in Fig. 14b, d, respectively. As illustrated in Fig. 14, for as-cast MG, the serrated flows are clearly observed. However, for the MP and LP surfaces, the serrated flows have been significantly suppressed, which shows a high consistency with the elimination of shear bands. This phenomenon is attributed to the kinetic limitation of shear bands [39]. On the as-cast MG surface, a single shear band can accommodate the imposed plastic deformation, resulting in the formation of serrated flows. In contrast, on the MP and LP surfaces, the introduction of the secondary phase (ZrN) could hinder the propagation of a single shear band and promote the operation of multiple shear bands, thereby resulting in smooth load-depth

curves. The above analysis about shear bands and serrated flows indicates that the variation of the micro-scale plastic deformation of the MP and LP surfaces should be related to the introduction of the ZrN phase [40, 41].

3.6 Comparison of MP and LP

Combined with the above analysis, the performance of the laser-nitrided surfaces treated by MP and LP in terms of surface roughness, surface porosity, and surface hardness as well as plastic deformation is systematically investigated, and the corresponding quantitative results are listed in Table 3. It is observed that LP can achieve lower surface roughness, higher processing efficiency, and similar surface hardness compared with MP, which indicates the advantages of LP over MP from the perspective of the surface quality and efficiency. In addition, LP as an environmentally friendly technique shows the potential to be the next-generation method for surface treatment.

4 Conclusions

In this paper, both MP and LP were performed for flattening the laser-nitrided Zr-based MG surfaces, and the surface hardness, together with plastic deformation of MP and LP surfaces, was analyzed as well. The obtained conclusions are as follows:

- (1) For surfaces A, B, and C treated by MP, the surface roughness is reduced to 0.109, 0.111, and 0.148 μm , and the reduction in surface roughness is 56.4%, 58.1%, and 44.6%, respectively. While for those processed by LP, the homogeneous surface morphologies are achieved with a remarkable reduction in surface roughness by 80.4% (from 0.250 to 0.049 μm), 81.5% (from 0.265 to 0.049 μm), and 74.2% (from 0.267 to 0.069 μm), respectively. This indicates that both MP and LP could effectively flatten the laser-nitrided surfaces, but LP performs better in terms of the reduction in surface roughness and improvement in surface quality.
- (2) The LP surfaces possess the slightly lower hardness than that of the MP surfaces, which should be owing to the dominant role of the laser thermal shock compared with the generation of the ZrN phase during LP.
- (3) The shear bands and serrated flows of the MP and LP surfaces have been significantly suppressed compared to as-cast MG, which demonstrates that the mechanism of micro-scale plastic deformation of the MP and LP surfaces has been changed.

Authors' contributions JH: investigation, methodology analysis and data curation and writing-original draft; LZ: validation, data curation,

writing-review and editing; ZZ: methodology, resources and validation; HH: supervision, resources, validation and writing-review; JY: resources and writing-review.

Funding This work was supported by the Natural Science Foundation of Jilin Province (20220101198JC), the National Natural Science Foundation of China (Grant No. 52075221), the Opening Project of the Key Laboratory of CNC Equipment Reliability, Ministry of Education, Jilin University (JLU-cncr-202208), and the Fundamental Research Funds for the Central Universities (2020–2022).

Data availability Data and materials are submitted as part of the manuscript.

Declarations

Ethics approval and consent to participate Not applicable.

Consent for publication Not applicable.

Consent to participate Not applicable.

Code availability Not applicable.

Competing interests The authors declare that they have no known competing financial interests or personal relationships that could have appeared to influence the work reported in this paper.

References

- Trexler MM, Thadhani NN (2010) Mechanical properties of bulk metallic glasses. *Prog Mater Sci* 55:759–839
- Chen MW (2011) A brief overview of bulk metallic glasses. *Npg Asia Mater* 3:82–90
- Khan MM, Nemati A, Rahman ZU, Shah UH, Asgar H, Haider W (2018) Recent advancements in bulk metallic glasses and their applications: a review. *Crit Rev Solid State* 43:233–268
- Inoue A, Wang XM, Zhang W (2008) Developments and applications of bulk metallic glasses. *Rev Adv Mater Sci* 18:1–9
- Schroers J (2013) Bulk metallic glasses. *Phys Today* 66:32–37
- Inoue A (2000) Stabilization of metallic supercooled liquid and bulk amorphous alloys. *Acta Mater* 48:279–306
- Jiang MQ, Dai LH (2009) On the origin of shear banding instability in metallic glasses. *J Mech Phys Solids* 57:1267–1292
- Dong J, Gao M, Huan Y, Feng YH, Liu W, Wang WH (2017) Enhanced tensile plasticity of Zr based bulk metallic glasses by a stress induced large scale flow. *J Alloy Compd* 727:297–303
- Hofmann DC, Suh JY, Wiest A, Duan G, Lind ML, Demetriou MD, Johnson WL (2008) Designing metallic glass matrix composites with high toughness and tensile ductility. *Nature* 451:1085–1089
- Chan CW, Lee S, Smith GC, Donaghy C (2017) Fibre laser nitriding of titanium and its alloy in open atmosphere for orthopaedic implant applications: investigations on surface quality, microstructure and tribological properties. *Surf Coat Technol* 309:628–640
- Ohtsu N, Yamane M, Kodama K, Wagatsuma K (2010) Surface hardening of titanium by pulsed Nd:YAG laser irradiation at 1064- and 532-nm wavelengths in nitrogen atmosphere. *Appl Surf Sci* 257:691–695
- Donaghy CL, McFadden R, Kelaini S, Carson L, Margariti A, Chan CW (2020) Creating an antibacterial surface on beta TNZT alloys for hip implant applications by laser nitriding. *Opt Laser Technol* 121:105793
- Zong X, Wang H, Li Z, Li J, Tang H (2020) Laser nitridation on Ti-6.5Al-35Mo-1.5Zr-0.3Si titanium alloy. *Surf. Coat Technol* 386:125425
- Hong J, Qian YF, Zhang L, Huang H, Jiang MQ, Yan JW (2021) Laser nitriding of Zr-based metallic glass: an investigation by orthogonal experiments. *Surf Coat Technol* 424:127657
- Huang H, Jiang MQ, Yan JW (2019) The coupling effects of laser thermal shock and surface nitridation on mechanical properties of Zr-based metallic glass. *J Alloy Compd* 770:864–874
- Chemkhi M, Reirant D, Roos A, Demangel C (2017) Role and effect of mechanical polishing on the enhancement of the duplex mechanical attrition/plasma nitriding treatment of AISI 316L steel. *Surf Coat Technol* 325:454–461
- Deng H, Hosoya K, Imanishi Y, Endo K, Yamamura K (2015) Electro-chemical mechanical polishing of single-crystal SiC using CeO₂ slurry. *Electrochem Commun* 52:5–8
- Chen C, Shu LS, Lee SR (2003) Mechano-chemical polishing of silicon wafers. *J Mater Process Tech* 140:373–378
- Liu DF, Yan RM, Chen T (2017) Material removal model of ultrasonic elliptical vibration-assisted chemical mechanical polishing for hard and brittle materials. *Int J Adv Manuf Tech* 92:81–99
- Fan ZH, Tian YB, Zhou Q, Shi C (2020) Enhanced magnetic abrasive finishing of Ti-6Al-4V using shear thickening fluids additives. *Precis Eng* 64:300–306
- Tian YB, Shi C, Fan ZH, Zhou Q (2020) Experimental investigations on magnetic abrasive finishing of Ti-6Al-4V using a multiple pole-tip finishing tool. *Int J Adv Manuf Tech* 106:3071–3080
- Zou YH, Xing BJ, Xu S (2020) Study on the magnetic abrasive finishing combined with electrolytic process-investigation of machining mechanism. *Int J Adv Manuf Tech* 108:1675–1689
- Deng T, Li J, Zheng Z (2019) Fundamental aspects and recent developments of metal surface polishing with energy beam irradiation. *Int J Mach Tool Manu* 148:103472
- Ma CP, Guan YC, Zhou W (2017) Laser polishing of additive manufactured Ti alloys. *Opt Laser Eng* 93:171–177
- Perry TL, Werschmoeller D, Li X, Pfefferkorn FE, Duffie NA (2009) Pulsed laser polishing of micro-milled Ti6Al4V samples. *J Manuf Process* 11:74–81
- Xu J, Zou P, Wang W, Kang D (2021) Study on the mechanism of surface topography evolution in melting and transition regimes of laser polishing. *Opt Laser Technol* 139:106947
- Deng TT, Li JJ, Zheng ZZ, Tian W, Li GL (2022) Influence of plasma beam polishing process parameters on surface roughness of AISI 304 stainless steel. *Appl Surf Sci* 585:152741
- Chang CS, Chen TH, Li TC, Lin SL, Liu SH, Lin JF (2016) Influence of laser beam fluence on surface quality, microstructure, mechanical properties, and tribological results for laser polishing of SKD61 tool steel. *J Mater Process Tech* 229:22–35
- Bordatchev EV, Hafiz A, Tutunea-Fatan OR (2014) Performance of laser polishing in finishing of metallic surfaces. *Int J Adv Manuf Tech* 73:35–52
- Krishnan A, Fang FZ (2019) Review on mechanism and process of surface polishing using lasers. *Front. Mech Eng* 14:299–319
- Li K, Zhao Z, Zhou H, Zhou H, Jin J (2020) Numerical analyses of molten pool evolution in laser polishing Ti6Al4V. *J Manuf Process* 58:574–584
- Reger NC, Balla VK, Das M, Bhargava AK (2017) Wear and corrosion properties of in-situ grown zirconium nitride layers for implant applications. *Surf Coat Technol* 334:357–364
- Liang W, Lu W, Xue Y, Zhang H, Fu H (2015) Nanoindentation response of laser shock peened Ti-based bulk metallic glass. *AIP Adv* 5:1947

34. Huang H, Jiang MQ, Yan JW (2018) Softening of Zr-based metallic glass induced by nanosecond pulsed laser irradiation. *J Alloy Compd* 754:215–221
35. Chen BQ, Pang SJ, Han PP, Li Y, Yavari AR, Vaughan G, Zhang T (2010) Improvement in mechanical properties of a Zr-based bulk metallic glass by laser surface treatment. *J Alloy Compd* 504S:S45–S47
36. Schuh CA, Hufnagel TC, Ramamurty U (2007) Mechanical behavior of amorphous alloys. *Acta Mater* 55:4067–4109
37. Ji G, Min S, Song N, Liao X, Guo S (2014) Improving the plasticity of bulk metallic glasses via pre-compression below the yield stress. *Mater Sci Eng A* 602:68–76
38. Huang H, Yan J (2017) Investigating shear band interaction in metallic glasses by adjacent nanoindentation. *Mater Sci Eng A* 704:375–385
39. Tang CG, Li Y, Zeng KY (2004) Characterization of mechanical properties of a Zr-based metallic glass by indentation techniques. *Mater Sci Eng A* 384:215–223
40. Fu J, Zhu YH, Zheng C, Liu R, Ji Z (2016) Effect of laser shock peening on the compressive deformation and plastic behavior of Zr-based bulk metallic glass. *Opt Laser Eng* 86:53–61
41. Cui X, Yu Z, Liu F, Du Z, Bai P (2019) Influence of secondary phases on crack initiation and propagation during fracture process of as-cast Mg-Al-Zn-Nd alloy. *Mater Sci Eng* 759:708–714

Publisher's note Springer Nature remains neutral with regard to jurisdictional claims in published maps and institutional affiliations.

Springer Nature or its licensor (e.g. a society or other partner) holds exclusive rights to this article under a publishing agreement with the author(s) or other rightsholder(s); author self-archiving of the accepted manuscript version of this article is solely governed by the terms of such publishing agreement and applicable law.